Biosensors and Bioelectronics 123 (2019) 185–194

Contents lists available at ScienceDirect

Biosensors and Bioelectronics

journal homepage: www.elsevier.com/locate/bios

A multidimensional impedance platform for the real-time analysis of single and combination drug pharmacology in patient-derived viable melanoma models

Diana Seidel[a], Rebecca Rothe[a], Mandy Kirsten[a], Heinz-Georg Jahnke[a], Konstantin Dumann[b], Mirjana Ziemer[b], Jan-Christoph Simon[b], Andrea A. Robitzki[a,*]

[a] Center for Biotechnology and Biomedicine (BBZ), Universität Leipzig, Division of Molecular Biological-Biochemical Processing Technology, Deutscher Platz 5, 04103 Leipzig, Germany

[b] Leipzig University Medical Center, Department of Dermatology, Venerology and Allergology, Philipp-Rosenthal-Str. 23, 04103 Leipzig, Germany

ARTICLE INFO

Keywords:
BRAF/MEK inhibitor synergy
Label-free drug kinetics
Multidimensional impedance spectroscopy
Patient-derived melanoma model
Real-time resistance monitoring

ABSTRACT

In today's development of anticancer drugs, there is an enormous demand for sensitive, non-invasive real-time screening technologies to identify pharmacodynamics/-kinetics of single and combined drugs with high precision. The combination of sophisticated drug sensitivity testing with advanced *in vitro* tumor models reflecting heterogeneous tumor behavior *in vivo* is needed to more reasonably predict therapeutic outcome *in vivo*.

In this study, the benefits of our real-time, non-invasive multidimensional impedance platform over standard *in vitro* drug sensitivity assays were demonstrated quantitatively using an advanced melanoma model. Detailed pharmacological profiles of clinically established targeted therapeutics in single and combination treatment have been identified in patient tissue and isolated 2D/3D cell line cultures. Impedance spectroscopy revealed significant differences in tissue structure responsible for BRAF inhibitor pharmacokinetics in $BRAF^{V600E}$ tumor microfragments and cell lines. Remarkably, BRAF-/MEK inhibitor combination treatment of direct patient-derived tissue, but not melanoma cell lines, resulted in short-term antagonistic effects consistent with *in vivo* findings. In contrast, the clinically validated resistance delay and thus long-term synergy of targeted therapeutics in advanced melanoma models has been demonstrated using impedance technology.

The results demonstrate limited clinical transferability of 2D/3D cancer cell line-based chemosensitivity data and underline the importance of *in vivo*-like direct patient-derived tissue for predictive drug studies. Our non-invasive and highly sensitive multidimensional impedance platform offers great potential for quantifying short- and long-term drug kinetics and synergies to identify the most effective drug combinations in advanced cancer models, thereby improving personalized drug development and treatment planning and ultimately, overall patient outcomes.

1. Introduction

In cancer research, the discovery of novel drugs is an extremely time- and cost-intensive process (McKim, 2010), especially as more than 95% of molecular entities fail in clinical trials because of toxicity and poor efficacy (Unger et al., 2014; Zanoni et al., 2016). Reasons are an inadequate simulation of *in vivo* tumor behavior due to the frequently applied 2D cancer models and a limited information gain about the drug-induced biological outcome through the use of standard assays in preclinical drug development (Eichler et al., 2015; Tanner and Gottesman, 2015).

To overcome biological drawbacks, current research focuses primarily on 3D cultures of cancer cell lines that capture key features of tumor tissue in terms of drug penetration, cell-cell and extracellular matrix (ECM) interaction, cell cycle alteration and activation of pathway signaling (Verjans et al., 2018; Zanoni et al., 2016). The use of patient-derived explants or cell models further enhances clinical relevance as acquired drug resistance and inter- and intra-tumor heterogeneity can be modeled (Das et al., 2015).

Equally important is the use of a reliable chemosensitivity assay and important pharmacological parameters as a prerequisite for accurate prediction of temporal and spatial drug activity. However, standard viability or metabolic activity analyzes, such as ATP or XTT assays, are cumbersome endpoint measurements that fail to reflect drug-induced

* Corresponding author.
E-mail address: andrea.robitzki@bbz.uni-leipzig.de (A.A. Robitzki).

https://doi.org/10.1016/j.bios.2018.08.049
Received 25 June 2018; Received in revised form 14 August 2018; Accepted 20 August 2018
Available online 23 August 2018
0956-5663/

changes in cell physiology, structure and microenvironment (Celli et al., 2014; Friedman et al., 2015). To counteract methodological limitations, electrochemical impedance spectroscopy (EIS) has been developed as a non-invasive, real-time, high-throughput chemosensitivity read-out technique with the ability to detect cytotoxicity (Kustermann et al., 2013), proliferation (Lei et al., 2014) and tissue structure changes (Jahnke et al., 2013, 2014) in various tumor entities.

In the analysis of drug activity in pre-clinical *in vitro* research, most studies focus mainly on IC_{50} values derived from dose response curves (Eldawud et al., 2014; Lei et al., 2018). However, this measure reflects only a small part of the pharmacokinetics and -dynamics of a substance and is less suitable for the analysis of drug combination treatments (Foucquier and Guedj, 2015; Santo et al., 2017).

Therefore, this study focuses on a subset of drug pharmacology parameters including the maximum efficacy of substances and their synergistic potential that are needed to assess short- and long-term therapeutic success, taking into account resistance development and tumor relapse (Cortés-Ciriano and Bender, 2016; Han et al., 2017).

To overcome the technical limitations in cancer drug discovery, we developed a multielectrode (MEA) and microcavity (MCA)-based multidimensional impedance platform for quantitative, non-invasive and real-time pharmacokinetics and -dynamics analysis of single and combined MAPK-targeting therapeutics in sensitive $BRAF^{V600E}$ melanoma models. While several studies have already described a specific impedimetric behavior of drug-treated cell line monolayers and spheroids (Eichler et al., 2015; Poenick et al., 2014), this work focuses for the first time on the comparison of original patient tumor tissue with derived 2D and 3D cell cultures to evaluate transferability of cell model data to the *in vivo* situation. The application of our impedimetric screening technique and drug activity-related parameters to patient-derived undissociated melanoma tissue aims to improve the predictability of combined targeted cancer therapy *in vivo* by *in vitro* generated chemosensitivity data. Predicting short- and long-term drug synergies *ex vivo* provides major benefits for developing successful personalized therapy regimes and ultimately improving melanoma patient prognosis.

2. Material and methods

For detailed procedure, please refer to Supplementary Methods.

2.1. Patient-derived melanoma cultures

Viable patient-derived tumor tissue was obtained from excisions of cutaneous melanoma specimens. All methods were performed in accordance to the Declaration of Helsinki with local ethics committee approval (Leipzig University Medical Centre; No. 224-11-11072011 and No. 208-16ek). Written informed consent was always obtained from each patient. For cell model origin, see Supplementary Table S1.

2.2. Targeted therapeutics

Vemurafenib (PLX-4032; V-2800), dabrafenib (GSK2118436: D-5678), trametinib (GSK1120212: T-8123) all from LC Laboratories. Encorafenib (LGX818: A13226), cobimetinib (GDC-0973: A11441), binimetinib (MEK162: A11493) all from Adooq.

2.3. ATP assay

Cell viability was quantified using the ATPLite Luminescence Assay System (Perkin Elmer).

2.4. DNA mutational analysis

Mutation status of typical melanoma driver genes (BRAF, NRAS, KIT, MAP2K1) was characterized. Primers are listed in Supplementary Table S2.

2.5. Molecularbiological assays

Melanoma tissue structure and marker expression was analyzed using immunocytochemistry. For applied antibodies, refer to Supplementary Table S3.

2.6. EIS

For substance screening on melanoma monolayers, cells were seeded on our self-produced 9-well interdigital electrode (9wIDE) arrays (Haas et al., 2010). For measurement, 9wIDE MEAs were inserted into our self-developed multiplexer board, which was connected to an Agilent 4294 A high-precision impedance analyzer (Agilent Technologies, USA). Impedance spectra (500 Hz to 5 MHz, 51 points, 10 mV amplitude) of cells before and after drug application were recorded with our self-developed software IMAT v2.2.5.3 for 96 h. For all experiments, controls from the same cell line/passage (2D/3D) or tumor specimen (TMFs) were included. Control samples were treated with the solvent of drug stocks (dimethyl sulfoxide, DMSO) in an appropriate amount (final dilution on cells: 0.1 – 0.2%). Blank values of cell-free 9wIDE MEAs were determined. Per experiment and condition, impedance of 5–7 electrodes was analyzed.

For drug testing on spheroids and TMFs, our self-developed microcavity array (MCA) with pyramidal cavities (edge length 400 µm) was used in combination with the above mentioned impedance measurement platform (Krinke et al., 2010). Impedance spectra (5 kHz to 5 MHz, 51 points, 100 mV amplitude) were recorded before drug administration (day 0) and thereafter every day or every three days. Per experiment and condition, six spheroids/TMFs were used. A viability staining was performed on completed experiments.

Data analysis was done with the self-developed IDAT software v3.6.3, which calculates a relative impedance spectrum $|Z|_{rel}$ (%) $= ((|Z|_{covered} - |Z|_{blank})/|Z|_{blank} \times 100)$ and determines its maximum. Time traces of the relative impedance maximum were normalized to the starting point of the experiment and the controls. In order to assess the influence of tissue structures on relative impedance, the frequency at impedance maximum and the impedance at 5 MHz were analyzed.

2.7. Drug synergy analysis

Drug synergy was analyzed using the freeware CompuSyn 1.0 (combosyn.com/index.html) that is based on the combination index (CI) algorithm of Chou/Talalay (Chou and Talalay, 1984). Two drugs can have an antagonistic ($CI > 1$), additive ($CI = 1$), slightly synergistic ($0.7 < CI < 1$), synergistic ($0.3 < CI \leq 0.7$) or strongly synergistic ($0 < CI \leq 0.3$) mode of action. In clinical tumor treatment, the proportion of inhibited cells must be high in order to increase therapeutic success (Zhao et al., 2014). Thus, CIs at IC_{75} (concentration inducing an inhibition of 75% of cells) were used.

2.8. Statistical analysis

All statistical analyzes were performed using Graphpad Prism 5.0. Relative IC_{50} values were determined by nonlinear sigmoidal curve fitting. For drug kinetics, curve upper plateau and logarithmised IC_{50} values were plotted over time and fitted non-linearly. Drug kinetics were shown with 95% confidence intervals. All other values were shown as means ± s.e.m. Multiple group comparisons were done by a two-way ANOVA and Bonferroni post hoc test. Comparisons between two groups were analyzed by *t*-test. Differences between two means with $p < 0.05$ were considered significant (*), $p < 0.01$ very significant (**) and $p < 0.001$ highly significant (***). For monolayers and spheroids, four experiments were analyzed. For TMFs, 4–6 replicates per condition were shown.

Correlation coefficients (r^2) of multiple method data was determined applying two-tailed Pearson correlation and color-coded with

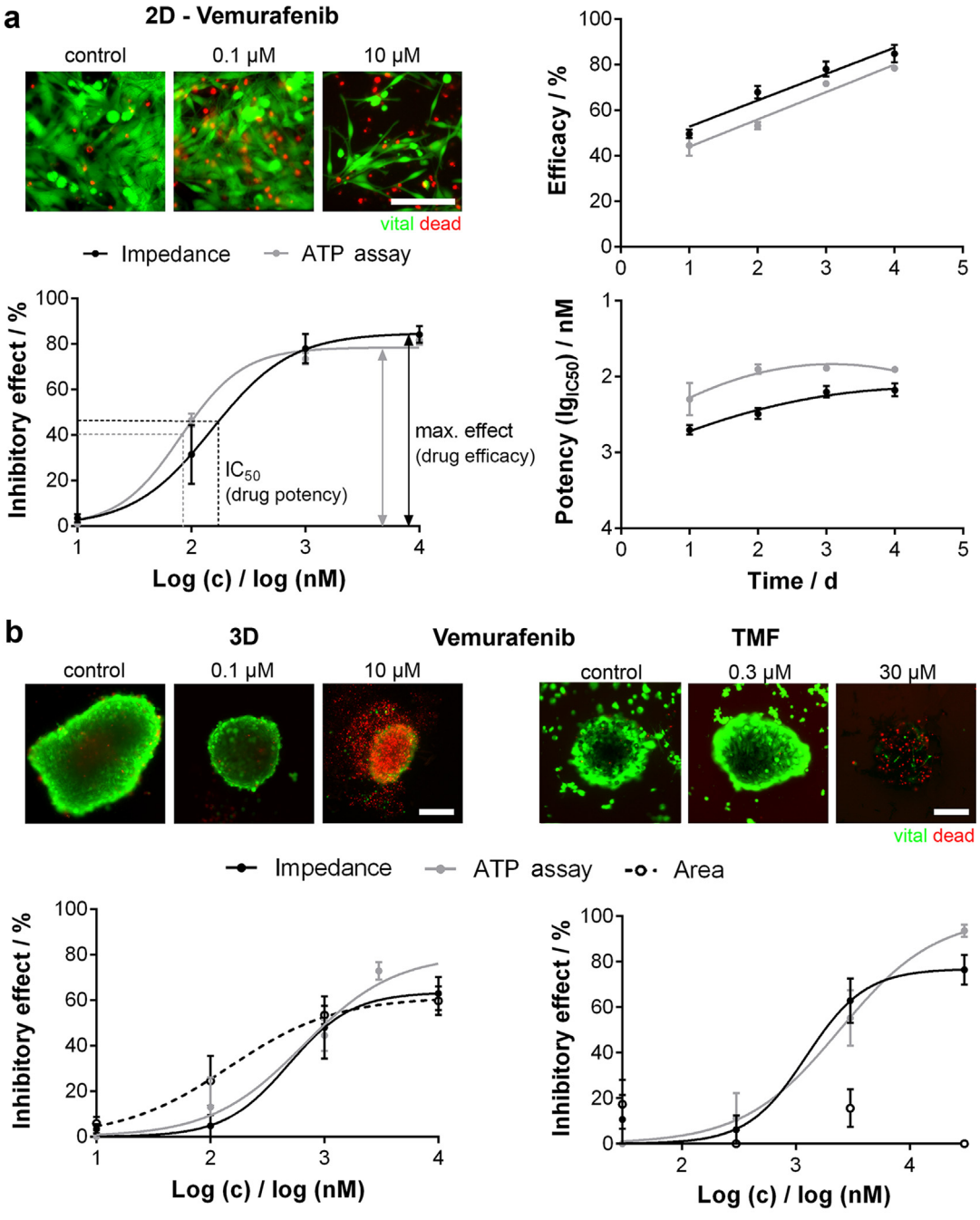

c

2D-Monolayer		3D-Spheroid				3D-Tumor Microfragment			
Impedance		**Impedance**		**Area**		**Impedance**		**Area**	
Efficacy	Potency	Efficacy	Potency	Efficacy	Potency	Efficacy	Potency	Efficacy	Potency
0.8987	0.9688	0.8385	0.9603	0.743	0.9074	0.8063	0.9999	0.01942	0.02286
ATP assay		**ATP assay**				**ATP assay**			
N = 11	16	8	8	8	8	24	32	24	32

Fig. 1. Impedance spectroscopy is an accurate measure of chemosensitivity and drug kinetics with highest correlation to standard ATP assay. BRAF inhibitor vemurafenib was applied to different BRAF mutated melanoma models. (**a**) Normalized concentration-response curves of a 2D cell line (left). Potency and efficacy plotted over time (right). (**b**) Concentration-response curves in 3D cell cultures (left) and tumor microfragments (TMF, right) applying the methods EIS, ATP assay and size detection (cross-section area). Viability stainings visualize drug effects. Scale bar 200 µm. (**c**) Correlation analysis. Highest correlation (black framed boxes). n = see figure.

red (rare: < 0.5), yellow (medium: 0.5–0.8), light green (strong: 0.8–0.95) and green (very strong: > 0.9).

For synergy analysis, CI values were calculated using the mean of replicate experiments to allow for a higher accuracy and were thus shown without standard error.

3. Results and discussion

3.1. Strong correlation of EIS and standard assay data of melanoma drug kinetics

As viability assays such as ATP measurement are widely used in *in vitro* drug development, advanced chemosensitivity analyzes should yield similar results to be applicable in this area.

Therefore, the activity of BRAF inhibitor vemurafenib was investigated in patient-derived $BRAF^{V600E}$ (2D and 3D cell lines) and $BRAF^{K601E}$ (tumor microfragments, TMF) melanoma using ATP quantification and impedance spectroscopy. For in-depth *in vitro* pharmacology analysis, efficacy (maximum inhibitory effect) and potency (IC_{50} value) were determined and plotted over time to reveal drug activity (Fig. 1a). For melanoma monolayers, concentration-response curves showed a similar progression for ATP assay and impedance data. No significant difference was observed between efficacy (ATP: 78.4 ± 2.1%; EIS: 84.8 ± 7.8%) and IC_{50} values (ATP: 80.5 ± 1.1 nM; EIS: 151.1 ± 1.47 nM). Underlining the measured data, the viability staining showed a decrease of viable cells and increase of dead cells in a concentration-dependent manner (Fig. 1a, left).

Besides pharmacological parameters, the kinetics of a drug are of major importance to assess its activity profile. The slope (linear regression) or half-life (non-linear regression) measures if an active substance enhances its activity over time. In combination, the y-axis intercept (linear regression) and the plateau (non-linear regression) provide information on general efficacy or potency. The pharmacokinetics of vemurafenib in 2D melanoma cells again showed a comparable progression for ATP assay and EIS data (Fig. 1a, right). The efficacy increased linearly during the four-day incubation period. For both methods, a constant slope of 12 and an insignificant variation of the y-intersect (ATP: 31.9 ± 4.3%; EIS: 41.2 ± 5.1%) were determined. Potency data followed a non-linear increase (decrease of logarithmised IC_{50}). Maximal potency was reached after two (ATP) and three days (EIS), respectively. Curves showed half-lives of 0.78 (ATP) and 1.77 days (EIS) and similar plateaus of 70.8 ± 1.2 nM (ATP) and 79.1 ± 1.8 nM (EIS).

For 3D cultures, ATP and impedance measurements were compared to the size of 3D cultures (expressed as change in cross-section area) (Fig. 1b, left). Viability staining of spheroids indicated a vemurafenib concentration-dependent decrease in size and viability. Concentration-response curves, in turn, showed similar IC_{50} values of ~ 550 nM for ATP assay and EIS data, while demonstrating a 3.5-fold increased potency for size measurement. A strongly reduced comparability of ATP assay and EIS data with 3D culture size was evident for TMF chemosensitivity analysis (Fig. 1b, right). Even with high drug effects that caused complete cell destruction (30 µM vemurafenib), 3D structures did not change size because of the substantial fraction of extracellular matrix in patient-derived non-dissociated tissue (see also Fig. 2; Supplementary Fig. S1). This result was also reflected in the concentration-response curves, where regression was not possible for size measurement, while ATP analysis and impedance data showed a similar progression.

To quantify the comparability of chemosensitivity methods in melanoma culture models, a correlation analysis was performed (Fig. 1c). Impedance and ATP assay data were highly correlative ($0.8 < r^2 < 1.0$), while the size showed moderate (spheroids: $0.7 < r^2 < 0.9$) or no correlation (TMF: $r^2 < 0.1$) to the standard ATP assay. Hereby, we prove for the first time the strong quantitative correlation of drug kinetics, which was determined by EIS and standard viability assay. Since results were independent of the applied cell/tissue culture model, we were also able to qualify our impedance platform for the use in industrial drug screening applications for the study of complex organotypic cultures such as TMFs.

3.2. Melanoma tissue structure-dependent differences in BRAF inhibitor sensitivity

Following quantitative validation for a meaningful in-depth pharmacokinetics analysis, impedance spectroscopy was used to identify culture model-dependent differences in BRAF inhibitor efficacy and potency over time. All cultures treated with BRAF inhibitor reacted non-linearly (Fig. 2; Supplementary Fig. S1). Highest efficacy was visible for 2D (100.4 ± 10.1%) and 3D cell cultures (89.0 ± 8.6%), whereas it was much lower for TMFs (67.5 ± 7.3%). Furthermore, half-life increased with the complexity of the culture form from 1.8 to 3.9 days (Fig. 2a, left).

If real impedimetric data of all tested BRAF inhibitors was compared among melanoma models at day three, highly significant differences were visible between 2D/3D cell line cultures and TMFs (Fig. 2b, left). At this early stage, potency of the three BRAF inhibitors also varied significantly between cultures, with TMFs always showing the highest IC_{50} values (lowest potency). Interestingly, the described effect turned at late incubation periods, when potency kinetics were fitted. While monolayers and TMFs had similar plateaus below 100 nM, spheroids were characterized by a decreasing drug potency over time and eventually reached a five-fold higher IC_{50} value (Fig. 2a, right). The described cell culture-dependent efficacy and potency developments were also evident for the use of other BRAF inhibitors (Supplementary Fig. S1a).

To identify the reason for the differing pharmacological parameters, tissue structure and composition were examined. Partial insensitivity to inhibitors and thus reduced overall efficacy in patient-derived organotypic TMFs was caused by their cellular heterogeneity. Fibroblast and endothelial marker CD90 staining showed expression in TMFs, but not isolated cell line cultures (Fig. 2e). Several studies confirm the effect of mixed cell cultures consisting of tumorous and non-tumorous as well as intrinsically resistant and sensitive cancer populations on drug efficacy (Santo et al., 2017; Tanner and Gottesman, 2015).

The diminished potency progression over time in spheroids was most likely triggered by a change in the number of available receptors (Srinivasarao et al., 2015). A diffusion study with Calcein-AM, which mimics the penetration of small-molecule BRAF inhibitors, showed only staining of the outer cell layer in spheroids (Fig. 2e). A gradual killing of cells in the periphery caused a shrinkage of the spheroid and thus the number of cells available to the drug (*i.e.* number of receptors). A high cell density in spheroid sections was also validated by DAPI staining. In contrast, TMFs were easily penetrated and showed loosely packed tissue consisting of cell islands interspersed by extracellular matrix made of Collagen I and N-Cadherin. Using tissue structure-specific impedance parameters, the visualized 3D cell organization was also quantitatively validated (Supplementary Fig. S2b). The shift of the relative impedance maximum to lower frequencies, and in particular the significantly higher relative impedance at 5 MHz, contrasted the homogeneous distribution of densely packed cells in spheroids with the irregular cell cluster arrangement in TMFs (Jahnke et al., 2013, 2014).

The identified half-life increase in complex tissue structures correlated with a strong expression of extracellular matrix molecules such as metastasis-specific N-Cadherin and dermis-abundant Collagen I (Fig. 2e). Several studies describe an absorption of active substances by extracellular matrix proteins and mechanical barriers as the main reasons for delayed drug-receptor binding. (Au et al., 2016; Seo et al., 2014; Theocharis et al., 2016).

The observed significant differences in BRAF inhibitor pharmacokinetics demonstrate the importance of patient-derived organotypic tissue models for drug discovery in *in vitro* pre-clinical research and

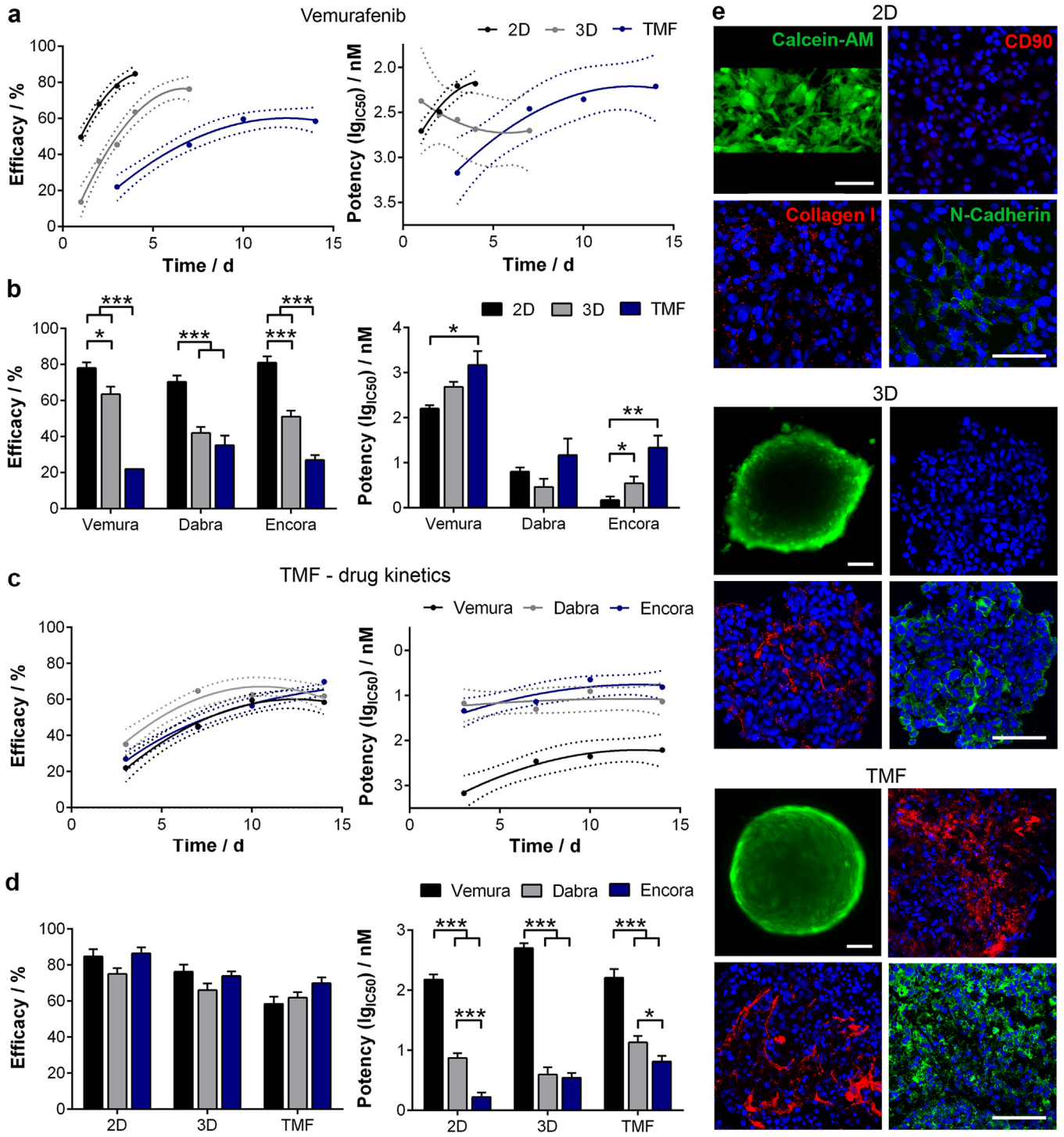

Fig. 2. Drug kinetics and efficiency are indicative for differences in melanoma model tissue structure. (**a**) Vemurafenib efficacy and potency kinetics in monolayer cells (2D), spheroids (3D) and tumor microfragments (TMF). (**b**) Efficacy and potency values of all BRAF inhibitors at treatment day 3. (**c**) Drug-dependent efficacy and potency kinetics in TMFs. (**d**) Drug-dependent pharmacology parameters at treatment day 4 (2D), 7 (3D) and 14 (TMF). (**e**) Calcein-AM penetration assay, staining of CD90, Collagen I and N-Cadherin in melanoma models. DAPI cell nuclei staining (blue). Scale bar 100 µm. vemurafenib (Vemura), dabrafenib (Dabra), encorafenib (Encora).

prove that 3D cell line cultures, unlike recent studies (Verjans et al., 2018; Zanoni et al., 2016), do not adequately reflect the human situation. In addition to the screening of active substances, impedance spectroscopy can be used to measure tissue organization. This broad application range is strongly superior to the read-out abilities of standard industrial chemosensitivity assays.

3.3. Comparability of in vitro and in vivo BRAF inhibitor pharmacokinetics in melanoma

In addition to the tissue properties affecting drug activity, the intrinsic potency and efficacy of each BRAF inhibitor were examined. In TMFs, all BRAF inhibitors showed similar efficacy plateaus of ~ 70% (Fig. 2c). However, dabrafenib by far developed the fastest half-effect

(2.6 days). These drug-specific efficacy patterns were also reproduced in the other melanoma models (Supplementary Fig. S1c). Consistently, no significant differences were observed in comparing the efficacies of BRAF inhibitors at highest activity (2D: 4 days; 3D: 7 days; TMF: 14 days), while potencies varied widely at these time points (Fig. 2d). Vemurafenib was characterized by the significantly highest IC_{50} data ranging from 150 to 500 nM, while encorafenib and dabrafenib showed comparable, 100-fold smaller values. Potency differences were also evident in the proportions of vital and dead cells in viability staining (Supplementary Fig. S1d).

The identified similar efficacies of all drugs justify their use in melanoma therapy for $BRAF^{V600}$ melanoma patients. In the clinic, the efficacy of a drug is fundamental as it indicates the proportion of cancer cells killed and cannot be easily predicted using drug potency (Whitebread et al., 2005). In contrast, potency is an essential measure of receptor specificity and therefore of safety pharmacology (Hennes et al., 2014). High-potency drugs achieve the same response at much lower concentrations than low-potency drugs and have an increased affinity for their given target, indicating a reduced risk of side effects (Chari, 2008). The clinically observed potencies of vemurafenib (31 nM) and dabrafenib (0.6 nM) and the concurrent significantly milder toxicity of dabrafenib in $BRAF^{V600}$ melanoma quantitatively prove the *in vitro* impedimetric pharmacokinetics and –dynamics. In this context, the novel BRAF inhibitor encorafenib showing enhanced efficacy and potency constitutes a valuable active substance for the treatment of specifically mutated BRAF in the future (Dummer et al., 2018).

3.4. Quantitative validation of drug synergies using impedance spectroscopy

Since tumor cells can easily adapt to targeted therapeutics through bypass survival signaling, current cancer treatment strategies focus primarily on the use of combinatorial agents to circumvent resistance formation (Gatzka, 2018). In this study, the efficacy of combined *versus* single drugs was assessed by synergy analysis. The combination index (CI) was used to quantify drug synergy over the entire range of action (Chou, 2010).

To validate the applicability of our impedance platform for drug combination studies, impedance and ATP assay data of BRAF-/MEK inhibitor co-treatment were compared in different melanoma models. For monolayer cells, impedance data showed synergistic behavior ($CI \leq 0.7$) until 70% of cells were inhibited (Fig. 3a). For higher fractions affected, additive to antagonistic BRAF-/MEK inhibitor behavior was detected. ATP assay data indicated an additive effect ($CI \sim 1$) over the complete concentration range.

In cancer therapy, synergistic behavior should ideally be determined for high levels of inhibited cells, guaranteeing near complete destruction of the tumor. Synergistic effects for small amounts of affected cells are not clinically relevant, as this promotes a relapse of cancer (Zhao and Bader, 2017). Therefore, CI values of impedance and ATP assay data were contrasted at 75% of inhibited cells (IC_{75}, concentration affecting 75% of cells) over time (Fig. 3b). Both methods showed comparable CI values of additive drug behavior, with the greatest divergence on day two (CI_{ATP}: 1.1; CI_{EIS}: 0.73). A similar but more synergistic CI progression was observed for spheroids co-treated with vemurafenib and cobimetinib (CI_{ATP}: 0.18, strong synergy; CI_{EIS}: 0.77, slight synergy) (Fig. 3c). In contrast, TMFs receiving BRAF-/MEK inhibitor co-treatment showed a reversed trend from strong antagonistic to additive behavior for high levels of affected cells (CI_{ATP}: 1.66; CI_{EIS}: 1.34) (Fig. 3d). These results demonstrated a sensitive characterization of drug synergy using impedance spectroscopy and ATP assay. In contrast, synergy classification was not possible by simple viability staining that showed no changes in viable and dead cell proportions when comparing single and combined drug treatment (Fig. 3a, c, d).

To validate impedance spectroscopy for drug synergy studies, a quantitative correlation analysis with ATP assay data was performed (Fig. 3e). Irrespective of the melanoma model used, a high correlation was found between the two chemosensitivity methods ($0.85 < r^2 < 0.98$), indicating the suitability of impedance spectroscopy for advanced drug combination analysis in *in vitro* pre-clinical pharmaceutical development. Reviewing the applicability of EIS for co-treatment studies is of particular importance as combination therapies will become increasingly important in the future to overcome intrinsic and acquired cancer resistance (Herbst et al., 2018; Ribas and Wolchok, 2018).

3.5. Sharp differences of short-term drug synergy in ex vivo and in vitro models

Based on the promising performance in drug combination analysis, impedance spectroscopy was used to assess the combined potential of BRAF-/MEK inhibitors in the advanced patient-derived melanoma model. The combination index of vemurafenib/cobimetinib at IC_{75} was plotted over time (Fig. 4a). While monolayer ($0.76 < CI < 1.05$) and spheroid cell line cultures ($0.29 < CI < 0.82$) exhibited quite constant combination indices of additive and synergistic behavior throughout the treatment period, TMFs were characterized by drug antagonism ($1.17 < CI < 2.2$). The described BRAF-/MEK inhibitor activity patterns were specific for the culture forms and independent of the applied drug combination (Fig. 4b; Supplementary Fig. S2a, b). For strong antagonistic behavior, effects were also confirmed qualitatively by a decrease in dead and an increase in vital cells in the viability staining (Supplementary Fig. S2b, top). In contrast, synergism led to a pronounced decrease in 3D culture size (Supplementary Fig. S2b, bottom).

Comparing melanoma models on the third day of treatment for various drug combination effects, 2D/3D melanoma cell cultures reacted synergistic, while melanoma patient tissue showed antagonism (Fig. 4c). The lack of synergy of encorafenib/binimetinib and dabrafenib/trametinib after short-term incubation was due to an already substantial activity of the individual treatments, so that the combination treatment could not increase effects (Supplementary Fig. S2a, right). Data indicated that the activity of co-treatment depended on complexity of the cultures. Even at the time of maximum drug effects, 2D cultures were characterized mainly by additive BRAF-/MEK inhibitor behavior ($0.69 < CI < 1.32$), spheroids exhibited synergistic drug response ($0.26 < CI < 0.81$) and TMFs ($1.59 < CI < 3.78$) retained an antagonistic reaction regardless of the BRAF-/MEK inhibitor combination used (Fig. 4d).

Beyond synergy potential analysis, impedance spectroscopy was used to assess the efficacy and potency of BRAF-/MEK inhibitor combinations. While combined treatments had similar efficacy levels in the respective melanoma models, potency (IC_{50} values) varied significantly (Fig. 4e; Supplementary Fig. S2c). As already observed in the individual treatments, vemurafenib/cobimetinib had the lowest overall potency. In cell line cultures, encorafenib/binimetinib and dabrafenib/trametinib achieved a 7-fold and 20-fold potency increase compared to the latter. Only TMFs were characterized by an insignificant difference in activity between encorafenib/binimetinib and dabrafenib/trametinib treatment and a low 3-fold potency gain of the latter over vemurafenib/cobimetinib, making all combinations a valuable choice for melanoma therapy. In the clinic, the impedimetrically observed similar activities of targeted drug combinations in organotypic cultures are reflected in comparable response rates and progression free survival (Eroglu and Ribas, 2016).

Considering the substantial melanoma model-dependent differences in combined BRAF-/MEK inhibitor efficiency, a clear need for more *in vivo*-like cultures in cancer drug research exists as therapeutics can have synergistic behavior in artificial cell models, whereas being antagonists *in vivo*. It is actually known from clinical research of BRAF- and MEK inhibitor combinations that drugs do not mutually reinforce each other during an acute treatment, but are able to slow down chronic resistance

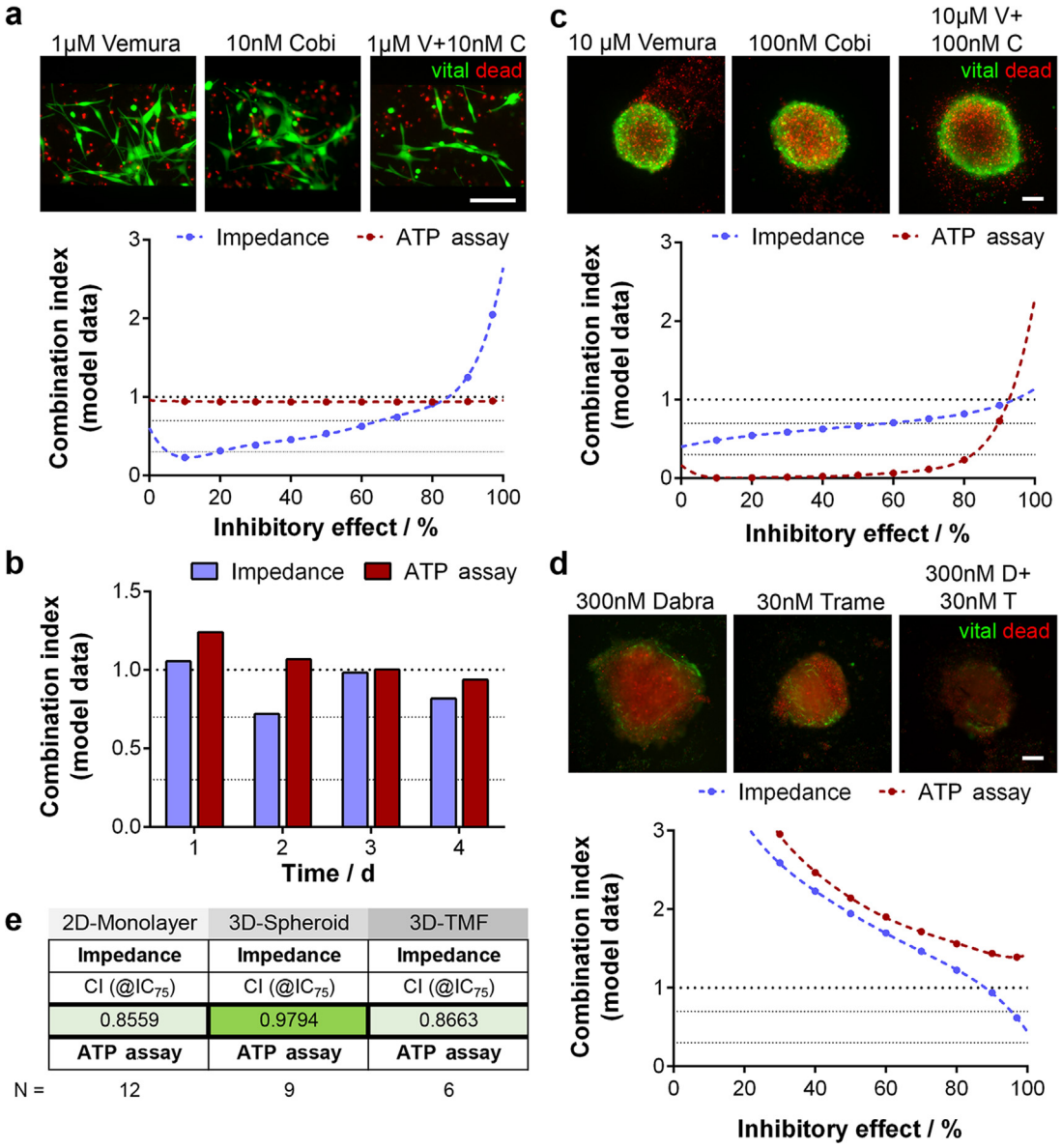

Fig. 3. EIS predicts BRAF-/MEK inhibitor synergy with high precision in all melanoma culture forms when compared to standard viability assay. Vemurafenib (Vemura, V) and cobimetinib (Cobi, C) synergy analysis in (**a**) 2D cultures. (**b**) Combinational indices (CI at IC_{75}) kinetics over time for 2D cultures. (**c**) Synergy analysis of V + C-treated spheroids (3D), and (**d**) dabrafenib (Dabra, D) and trametinib (Trame, T) synergy analysis in tumor microfragments (TMF). Combination index plotted against the inhibitory effect of the drug combination at day 4 (2D), 7 (3D) and 14 (TMF). Viability stainings visualize drug effects. Scale bar 100 µm. (**e**) CI correlation analysis. Highest correlation (black framed boxes). n = see figure.

emergence (Flaherty et al., 2012; Larkin et al., 2014). With our melanoma microfragment-based impedance technology, we provide a highly sensitive platform that allows the chemosensitivity analysis of viable excised tumor entities independent of the melanoma grade (level of skin depth) or stage (primary tumor, node, and metastasis).

3.6. Impedimetric resistance monitoring of single and combined BRAF-/MEK inhibitors

To validate the known clinical effect of delayed resistance emergence through BRAF-/MEK inhibitor combination treatment, cellular impedance was recorded of patient-derived melanoma spheroids treated with dabrafenib/trametinib alone or in combination over 60 days. Micrographs and viability staining after day 7 acute treatment showed equally sized spheroids with similar levels of viable and dead cells, regardless of the treatment regime (Fig. 5a). Prolonged incubation with dabrafenib for 60 days led to a sharp increase in spheroid size and viable cell number, while trametinib and the combined treatment resulted in a constant but significantly lower 3D culture diameter (69.9 ± 6.3% and 72.8 ± 12.2%) and a low level of vital cells (Fig. 5b, right).

Being able to measure tissue structure and ECM alterations that are known to accompany resistance emergence (Afasizheva et al., 2016; Hirata et al., 2015), EIS revealed significant differences for not only dabrafenib (122.3 ± 13.1%), but also trametinib (110.5 ± 9.5%) *versus* combined drug (61.5 ± 8.7%) chronic application. More strikingly, comparable temporal resistance emergence patterns were identified for the other BRAF-/MEK inhibitor single and combination treatments (Supplementary Fig. S3a).

Comparable to clinical findings, these results again demonstrate the advantages of impedance spectroscopy over standard industrial endpoint measurements for real-time monitoring of resistance emergence in patient-derived cell line spheroids. Because TMFs remain viable in *ex vivo* cultures for more than 100 days (Supplementary Fig. S3b), these

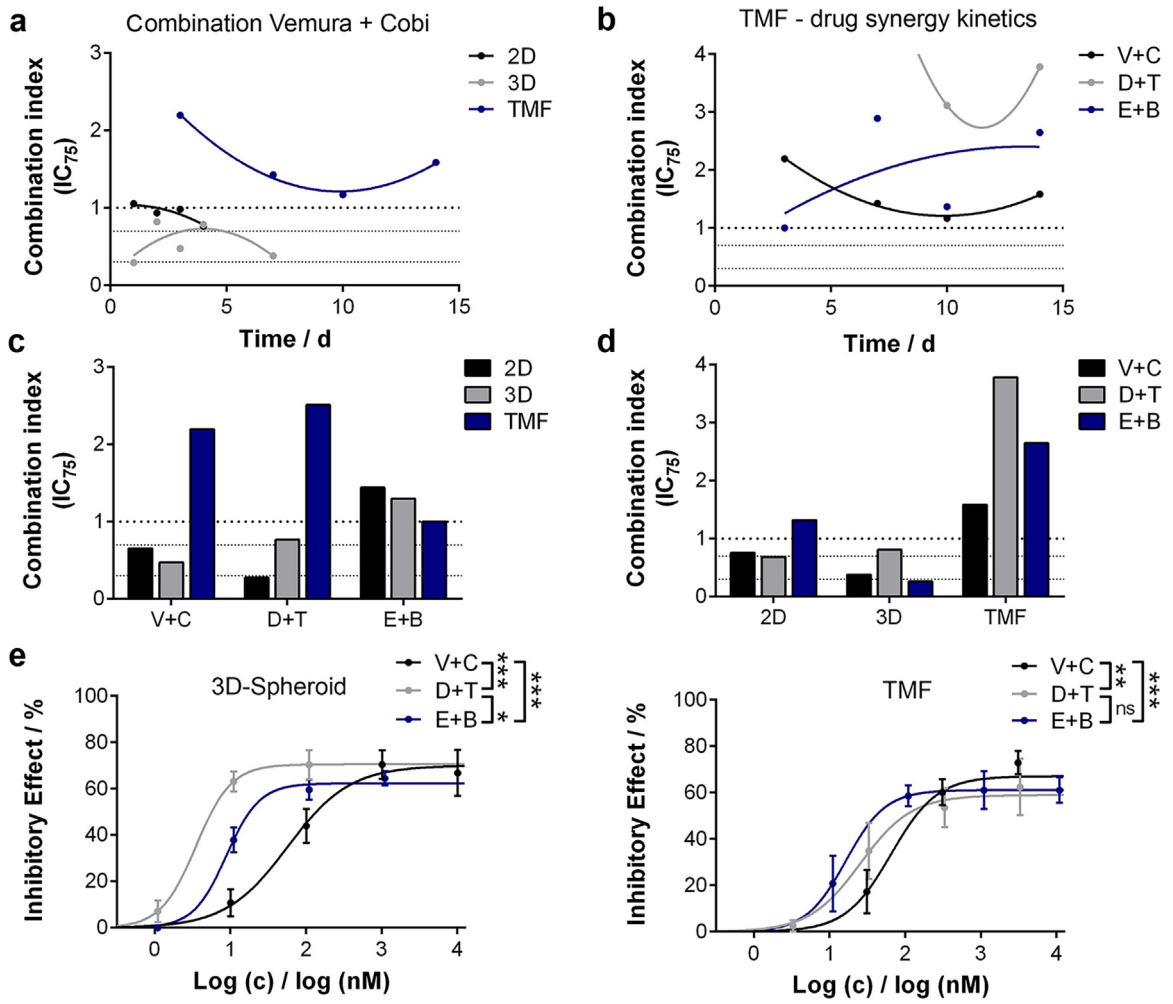

Fig. 4. Antagonistic-additive effects of BRAF-/MEK inhibitors on $BRAF^{V600E}$ TMFs are different from synergistic-additive actions in artificial 2D/3D melanoma cell models. (**a**) Combination index (CI) kinetics of vemurafenib/cobimetinib (Vemura + Cobi, V + C) treatment and (**b**) kinetics of all BRAF/MEK inhibitor combinations in tumor microfragments (TMF) measured with EIS. (**c**) At day 3 and (**d**) drug screening end, CIs of combination treatments at IC_{75} are compared. (**e**) EIS concentration-response curves in spheroids (day 7) and TMFs (day 14) with significant differences in potency (IC_{50} values). dabrafenib/trametinib (D + T), encorafenib/binimetinib (E + B).

organotypic tissue models are of considerable interest in conducting relevant studies of *in vivo* resistance development.

4. Conclusion

Here, we described for the first time the use of our self-developed multidimensional impedance platform for an in-depth pharmacology analysis of targeted therapeutics in an advanced patient-derived melanoma model. The quantified close correlation of ATP assays with impedimetrically obtained pharmacokinetics and –dynamics prove the high value of sensitive and non-invasive real-time EIS for pharmacological screenings of single drugs and combinations in short- and long-term setups. Moreover, substantial differences in drug response patterns between organotypic *ex vivo* and artificial *in vitro* 2D/3D cell cultures highlight the importance of *in vivo*-like cell models in drug development. This is particularly true since clinically observed responses to BRAF-/MEK inhibitors were very similar to the results of this study for TMFs. Superior to standard industrial assays, impedance spectroscopy is not only able to measure chemosensitivity patterns with high precision in a non-invasive and real-time manner, but also to identify tissue structure changes.

Several studies show the successful *ex vivo* culture of different patient-derived cancerous tissues such as head and neck squamous cell carcinoma (Kross et al., 2008), colorectal cancer (Weeber et al., 2015) and glioblastoma (Hubert et al., 2016), making the platform a valuable choice for the chemosensitivity analysis of various tumor entities. To be even more significant for pharmaceutical screenings, the microcavity prototype is currently scaled to a 96-well microtiter plate-assisted impedance platform for an automated, standardized and paralleled analysis of cancer therapeutics on *in vivo*-like TMFs.

Acknowledgement

This work was funded by the Ministry for Science and Culture of Saxony (SMWK; Elek-Indi-Mel; No. 100261990). Impedance analyzer, confocal microscope, and clean room equipment were funded by the State of Saxony and the European Union (SMWK/EFRE).

Competing interest statement

None.

Declarations of interest

None.

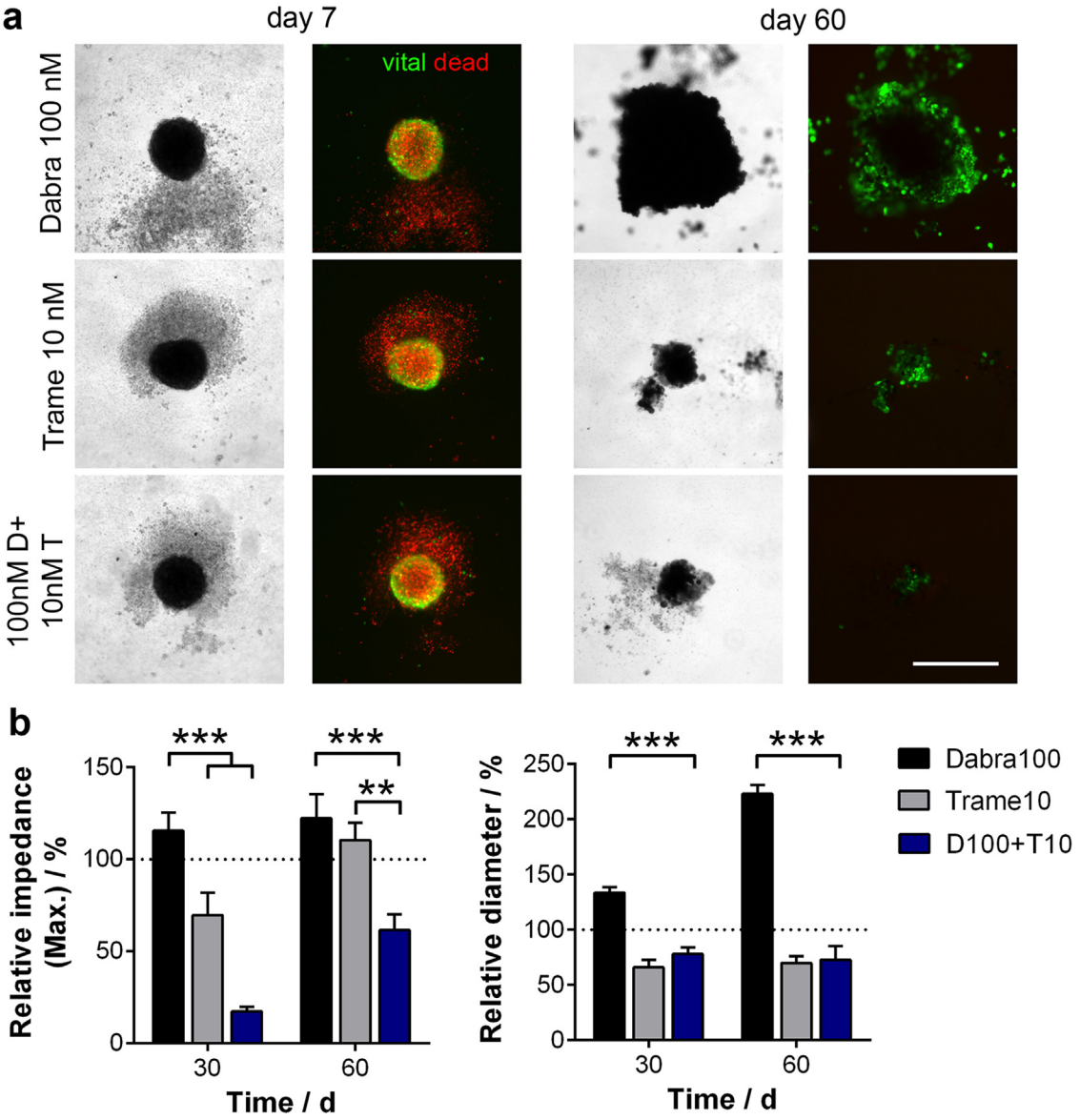

Fig. 5. Real-time monitoring of BRAF/MEK inhibitor-induced resistance in combination and single drug applications on $BRAF^{V600E}$ melanoma spheroids (**a**) Micrographs and viability stainings of spheroids after dabrafenib (Dabra, D) and trametinib (Trame, T) treatment alone and in combination. Partial missing viability staining in long-term treated spheroids due to melanin-induced blackening of cells and quenching of fluorescence. Scale bar 500 µm. (**b**) EIS and spheroid size data of long-term D/T (100 nM/10 nM) single and combination treatment normalized to acute effects (day 7, dashed line).

Appendix A. Supporting information

Supplementary data associated with this article can be found in the online version at doi:10.1016/j.bios.2018.08.049.

References

Afasizheva, A., Devine, A., Tillman, H., Fung, K.L., Vieira, W.D., Blehm, B.H., Kotobuki, Y., Busby, B., Chen, E.I., Tanner, K., 2016. BMC Cancer 16, 186.

Au, J.L., Yeung, B.Z., Wientjes, M.G., Lu, Z., Wientjes, M.G., 2016. Adv. Drug Deliv. Rev. 97, 280–301.

Celli, J.P., Rizvi, I., Blanden, A.R., Massodi, I., Glidden, M.D., Pogue, B.W., Hasan, T., 2014. Sci. Rep. 4, 3751.

Chari, R.V., 2008. Acc. Chem. Res. 41, 98–107.

Chou, T.C., Talalay, P., 1984. Adv. Enzym. Regul. 22, 27–55.

Chou, T.C., 2010. Cancer Res. 70, 440–446.

Cortés-Ciriano, I., Bender, A., 2016. ChemMedChem 11, 57–71.

Das, V., Bruzzese, F., Konecny, P., Iannelli, F., Budillon, A., Hajduch, M., 2015. Drug Discov. Today 20, 848–855.

Dummer, R., Ascierto, P.A., Gogas, H.J., Arance, A., Mandala, M., Liszkay, G., Garbe, C., Schadendorf, D., Krajsova, I., Gutzmer, R., Chiarion-Sileni, V., Dutriaux, C., de Groot, J.W.B., Yamazaki, N., Loquai, C., Moutouh-de Parseval, L.A., Pickard, M.D., Sandor, V., Robert, C., Flaherty, K.T., 2018. Lancet Oncol. 19, 603–615.

Eichler, M., Jahnke, H.G., Krinke, D., Muller, A., Schmidt, S., Azendorf, R., Robitzki, A.A., 2015. Biosens. Bioelectron. 67, 582–589.

Eldawud, R., Stueckle, T.A., Manivannan, S., Elbaz, H., Chen, M., Rojanasakul, Y., Dinu, C.Z., 2014. Biosens. Bioelectron. 59, 192–199.

Eroglu, Z., Ribas, A., 2016. Ther. Adv. Med Oncol. 8, 48–56.

Flaherty, K.T., Infante, J.R., Daud, A., Gonzalez, R., Kefford, R.F., Sosman, J., Hamid, O., Schuchter, L., Cebon, J., Ibrahim, N., Kudchadkar, R., Burris 3rd, H.A., Falchook, G., Algazi, A., Lewis, K., Long, G.V., Puzanov, I., Lebowitz, P., Singh, A., Little, S., Sun, P., Allred, A., Ouellet, D., Kim, K.B., Patel, K., Weber, J., 2012. N. Engl. J. Med. 367, 1694–1703.

Foucquier, J., Guedj, M., 2015. Pharmacol. Res. Perspect. 3, e00149.

Friedman, A.A., Letai, A., Fisher, D.E., Flaherty, K.T., 2015. Nat. Rev. Cancer 15, 747–756.

Gatzka, M.V., 2018. Cancers (Basel) 10.

Haas, S., Jahnke, H.G., Glass, M., Azendorf, R., Schmidt, S., Robitzki, A.A., 2010. Lab Chip 10, 2965–2971.

Han, K., Jeng, E.E., Hess, G.T., Morgens, D.W., Li, A., Bassik, M.C., 2017. Nat. Biotechnol. 35, 463–474.

Hennes, C., Batke, M., Bomann, W., Duhayon, S., Kosemund, K., Politano, V., Stinchcombe, S., Doe, J., 2014. Regul. Toxicol. Pharmacol. 70, 457–467.

Herbst, R.S., Morgensztern, D., Boshoff, C., 2018. Nature 553, 446–454.

Hirata, E., Girotti, M.R., Viros, A., Hooper, S., Spencer-Dene, B., Matsuda, M., Larkin, J., Marais, R., Sahai, E., 2015. Cancer Cell 27, 574–588.

Hubert, C.G., Rivera, M., Spangler, L.C., Wu, Q., Mack, S.C., Prager, B.C., Couce, M., McLendon, R.E., Sloan, A.E., Rich, J.N., 2016. Cancer Res. 76, 2465–2477.
Jahnke, H.G., Heimann, A., Azendorf, R., Mpoukouvalas, K., Kempski, O., Robitzki, A.A., Charalampaki, P., 2013. Biosens. Bioelectron. 46, 8–14.
Jahnke, H.G., Poenick, S., Maschke, J., Kendler, M., Simon, J.C., Robitzki, A.A., 2014. Cancer Res. 74, 6408–6418.
Krinke, D., Jahnke, H.G., Mack, T.G., Hirche, A., Striggow, F., Robitzki, A.A., 2010. Biosens. Bioelectron. 26, 162–168.
Kross, K.W., Heimdal, J.H., Olsnes, C., Olofsson, J., Aarstad, H.J., 2008. Scand. J. Immunol. 67, 392–399.
Kustermann, S., Boess, F., Buness, A., Schmitz, M., Watzele, M., Weiser, T., Singer, T., Suter, L., Roth, A., 2013. Toxicol. Vitr. 27, 1589–1595.
Larkin, J., Ascierto, P.A., Dreno, B., Atkinson, V., Liszkay, G., Maio, M., Mandala, M., Demidov, L., Stroyakovskiy, D., Thomas, L., de la Cruz-Merino, L., Dutriaux, C., Garbe, C., Sovak, M.A., Chang, I., Choong, N., Hack, S.P., McArthur, G.A., Ribas, A., 2014. N. Engl. J. Med. 371, 1867–1876.
Lei, K.F., Wu, M.H., Hsu, C.W., Chen, Y.D., 2014. Biosens. Bioelectron. 51, 16–21.
Lei, K.F., Liu, T.K., Tsang, N.M., 2018. Biosens. Bioelectron. 100, 355–360.
McKim Jr., J.M., 2010. Comb. Chem. High. Throughput Screen. 13, 188–206.
Poenick, S., Jahnke, H.G., Eichler, M., Frost, S., Lilie, H., Robitzki, A.A., 2014. Biosens. Bioelectron. 53, 370–376.
Ribas, A., Wolchok, J.D., 2018. Science 359, 1350–1355.
Santo, V.E., Rebelo, S.P., Estrada, M.F., Alves, P.M., Boghaert, E., Brito, C., 2017. Biotechnol. J. 12.
Seo, B.R., DelNero, P., Fischbach, C., 2014. Adv. Drug Deliv. Rev. 69–70, 205–216.
Srinivasarao, M., Galliford, C.V., Low, P.S., 2015. Nat. Rev. Drug Discov. 14, 203–219.
Tanner, K., Gottesman, M.M., 2015. Sci. Transl. Med. 7 (283ps289).
Theocharis, A.D., Skandalis, S.S., Gialeli, C., Karamanos, N.K., 2016. Adv. Drug Deliv. Rev. 97, 4–27.
Unger, C., Kramer, N., Walzl, A., Scherzer, M., Hengstschlager, M., Dolznig, H., 2014. Adv. Drug Deliv. Rev. 79–80, 50–67.
Verjans, E.T., Doijen, J., Luyten, W., Landuyt, B., Schoofs, L., 2018. J. Cell Physiol. 233, 2993–3003.
Weeber, F., van de Wetering, M., Hoogstraat, M., Dijkstra, K.K., Krijgsman, O., Kuilman, T., Gadellaa-van Hooijdonk, C.G., van der Velden, D.L., Peeper, D.S., Cuppen, E.P., Vries, R.G., Clevers, H., Voest, E.E., 2015. Proc. Natl. Acad. Sci. USA 112, 13308–13311.
Whitebread, S., Hamon, J., Bojanic, D., Urban, L., 2005. Drug Discov. Today 10, 1421–1433.
Zanoni, M., Piccinini, F., Arienti, C., Zamagni, A., Santi, S., Polico, R., Bevilacqua, A., Tesei, A., 2016. Sci. Rep. 6, 19103.
Zhao, J., Kelnar, K., Bader, A.G., 2014. PLoS One 9, e89105.
Zhao, J., Bader, A.G., 2017. Methods Mol. Biol. 1517, 115–126.